Supplement of Atmos. Chem. Phys., 26, 2965–2984, 2026
https://doi.org/10.5194/acp-26-2965-2026-supplement

Atmospheric Chemistry and Physics
Open Access
EGU

Supplement of

Disparate evolution mechanisms and optical absorption for transboundary soot particles passing through inland and sea pathways

Jian Zhang et al.

Correspondence to: Weijun Li (liweijun@zju.edu.cn)

S1. Change in prevailing winds and $PM_{2.5}$ concentrations

Figure S3 shows the change in hourly winds and $PM_{2.5}$ mass concentrations in the NCP and the YRD and the sea level pressure distribution in China during the observation period. The prevailing wind significantly changed from weak southern winds to strong northern winds in the NCP and the YRD on December 30, 2017 and December 7, 2020 under cold fronts (Figures S3a-b). On the same day, the average $PM_{2.5}$ concentration in the NCP rapidly decreased from 318 μg m^{-3} during the first observation period and 179 μg m^{-3} during the second observation period to 33 μg m^{-3} and 37 μg m^{-3} (Figures S3a-b). After 6-9 hours, the average $PM_{2.5}$ concentration in the YRD suddenly increased from 62 μg m^{-3} during the first observation period and 51 μg m^{-3} during the second observation period to 308 μg m^{-3} and 113 μg m^{-3} (Figures S3a-b). These results suggest that two typical transboundary transport events of pollutants from the NCP to the YRD occurred during the observation period.

S2. The classification of individual particles

Based on morphology and elemental compositions of particles, six basic types of aerosol components were classified as soot, mineral, S-rich, organic matter (OM), metal, and fly ash.

Soot particles are aggregation of many carbonaceous spheres (Figure 3a) and mainly contain C and minor O. Mineral particles mainly contain O, Si, and Al elements and present irregular shapes. S-rich particles, also called secondary inorganic aerosols, are mainly comprised of S, O, and N elements and generally are the mixtures of $(NH_4)_2SO_4$ and NH_4NO_3 (Li et al., 2016). OM particles mainly contain C, O, and Si and often exhibit near-spherical morphology or appear as coatings on S-rich particles. Metal and fly ash particles are mainly composed of O, Si, and metallic elements (e.g., Al and Fe) and present the morphology of single sphere or aggregation of several spheres.

Because we mainly focused on soot particles, individual particles were further classified into soot-containing, S-OM/metal/fly ash/mineral, S-rich, and OM/metal/fly ash/mineral particles based on their mixing states.

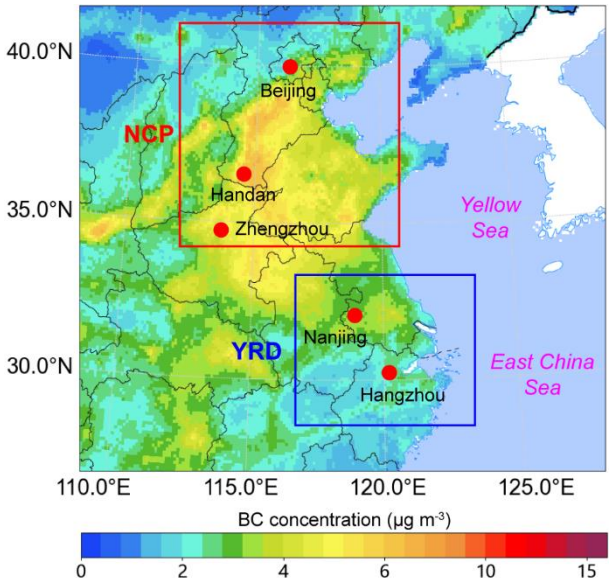

Figure S1. Spatial distribution of monthly averaged black carbon (BC) surface concentration in eastern China during December 2017 with the location of observation sites in the North China Plain (NCP) and the Yangtze River Delta (YRD) (http://tapdata.org.cn).

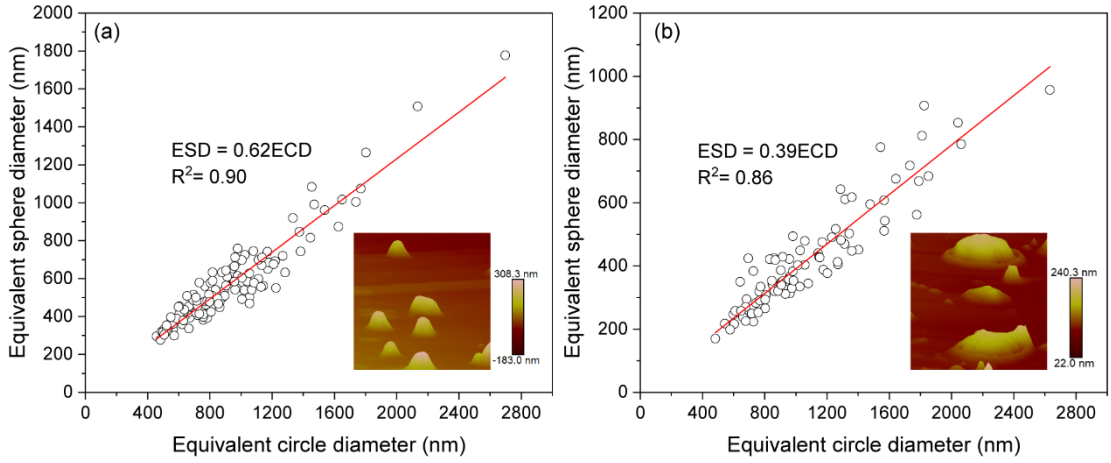

Figure S2. Linear correlation between the equivalent circle diameter (ECD) and the equivalent sphere diameter (ESD) of haze particles during two transboundary transport events. (a) Haze particles transported through the inland pathway. (b) Haze particles transported through the sea pathway. Typical atomic force microscopy (AFM) images of transported haze particles are displayed in the lower right corner in panels (a) and (b).

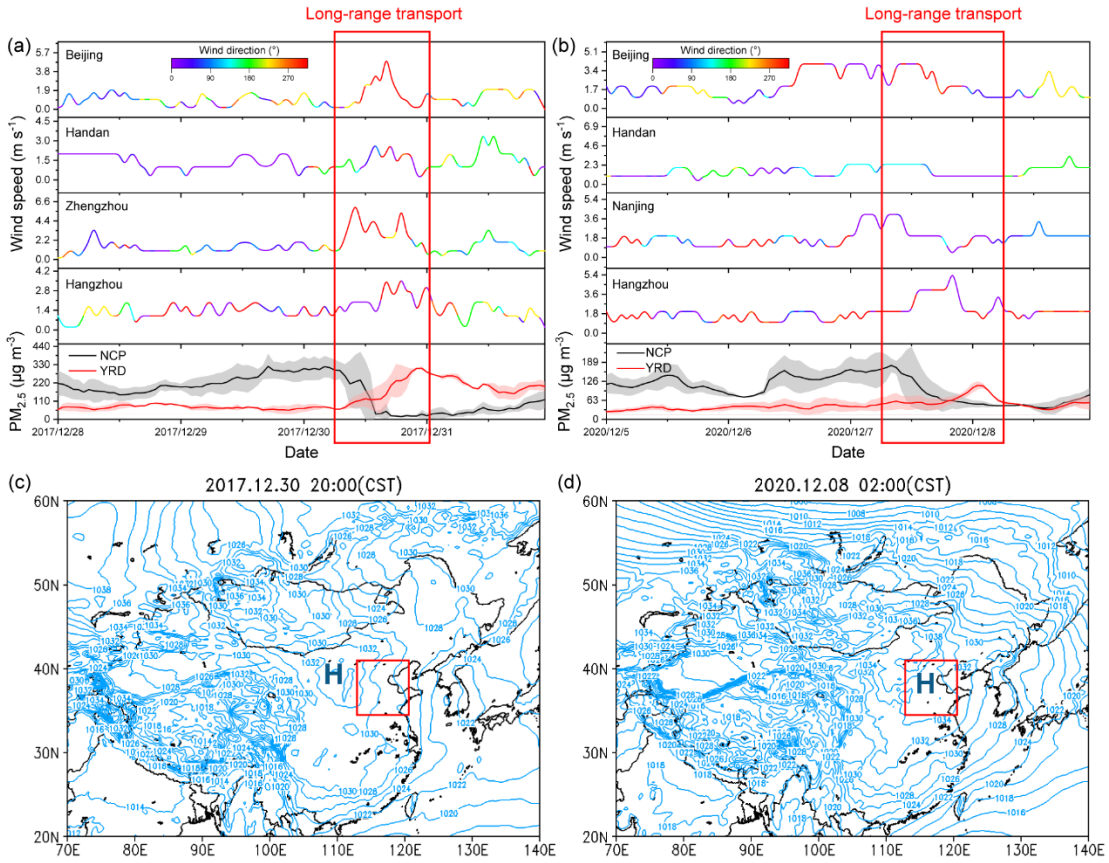

Figure S3. Time series of winds and $PM_{2.5}$ concentrations at different observation sites and sea level pressure distribution in China. (a) Winds and $PM_{2.5}$ concentrations during December 28-31, 2017. (b) Winds and $PM_{2.5}$ concentrations during December 5-8, 2020. (c) Sea level pressure distribution at 20:00 (local time) on December 30, 2017. (d) Sea level pressure distribution at 2:00 on December 8, 2020. Red rectangular boxes in panels (c) and (d) represent the NCP. CST is China local standard time; H is high pressure.

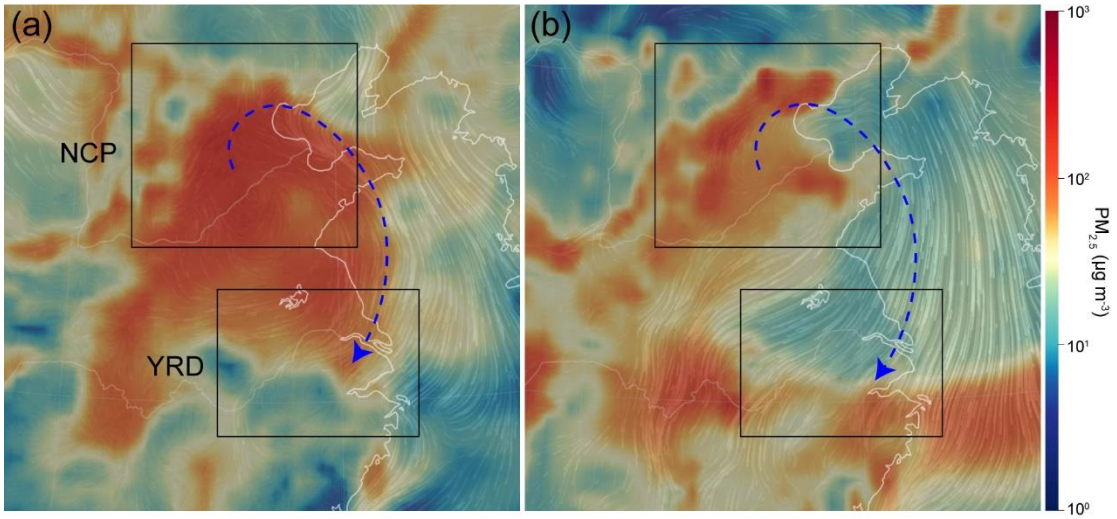

Figure S4. Wind fields combined with surface $PM_{2.5}$ concentrations in eastern China. (a) 11:00 (local time) on January 4, 2020. (b) 4:00 (local time) on February 8, 2021.

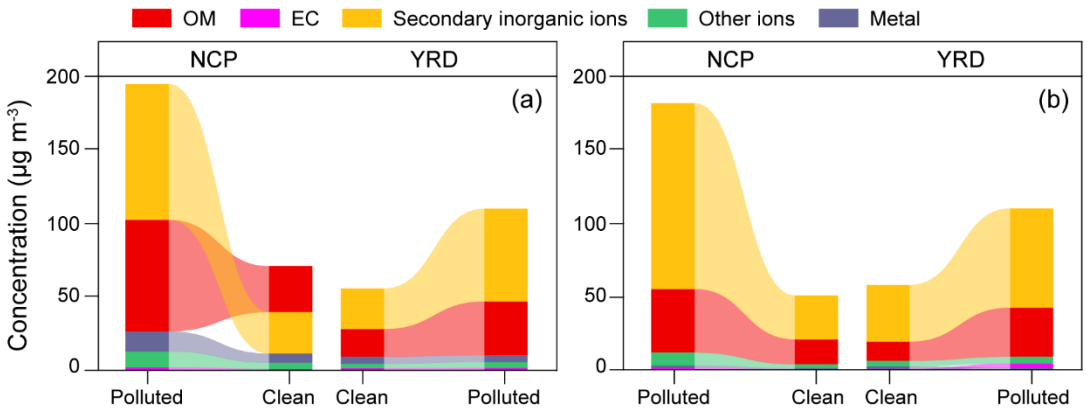

Figure S5. Variations in chemical compositions in $PM_{2.5}$ in the NCP and the YRD during two transboundary transport events. (a) Transportation through the inland pathway. (b) Transportation through the sea pathway.

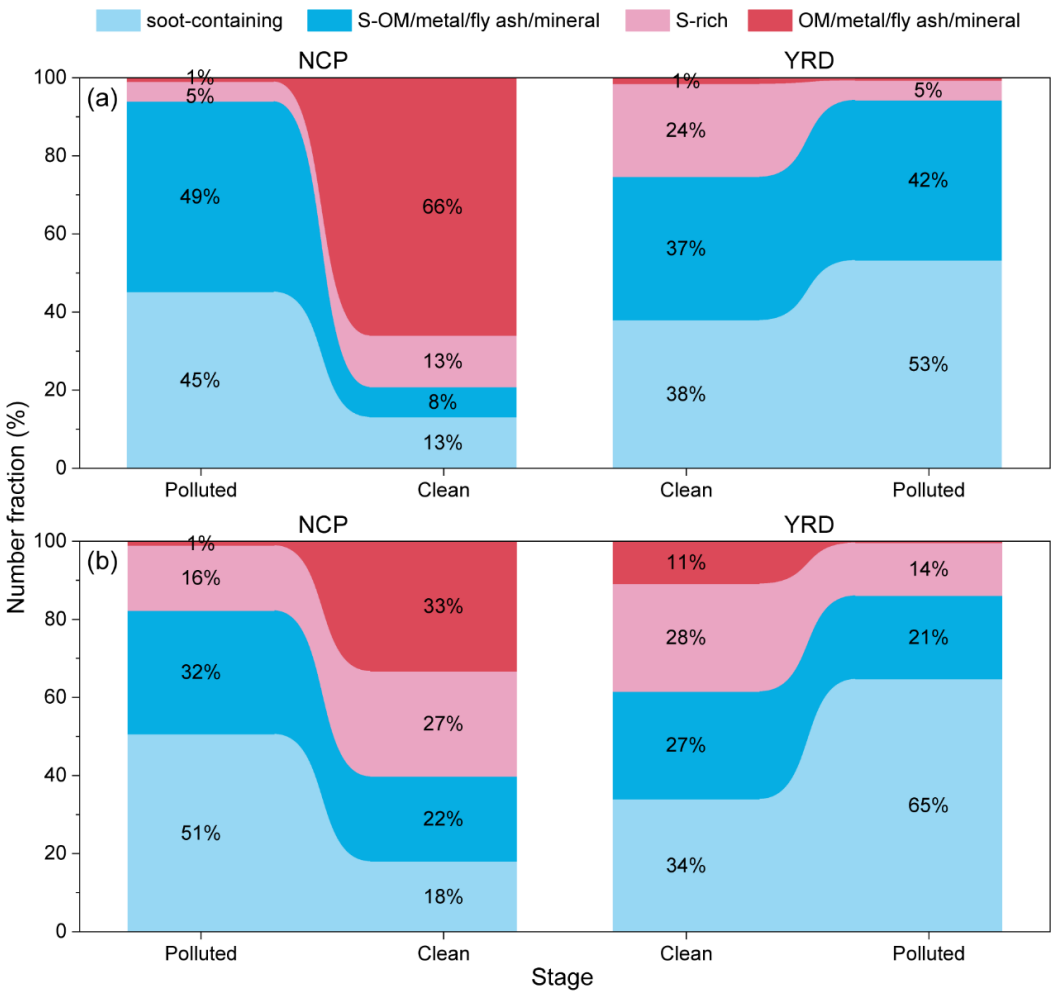

Figure S6. Variations in number fractions of individual particles in the NCP and the YRD during two transboundary transport events. (a) Transportation through the inland pathway. (b) Transportation through the sea pathway.

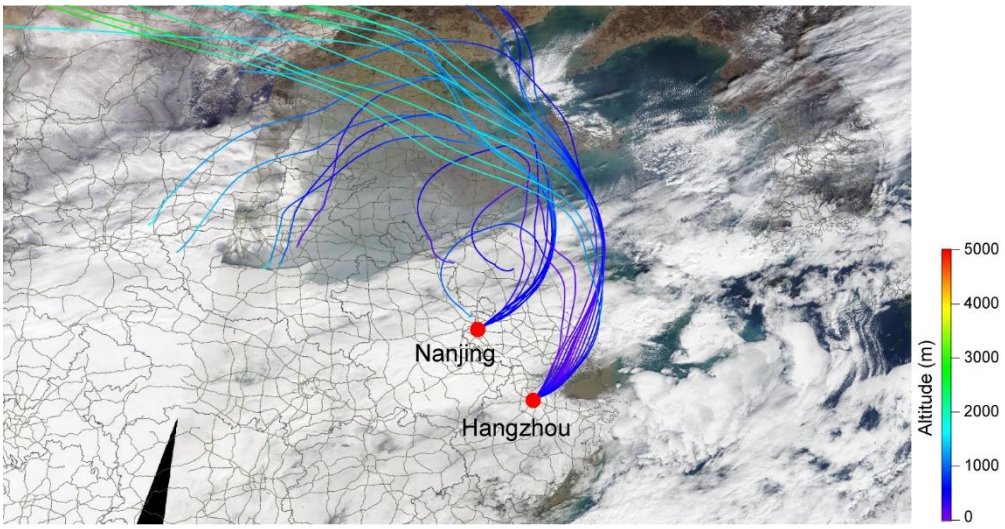

Figure S7. A satellite image combined with the backward trajectory of haze masses before arriving at Nanjing and Hangzhou sites during December 7-8, 2020. The satellite image is derived from NASA Worldview (https://worldview.earthdata.nasa.gov/).

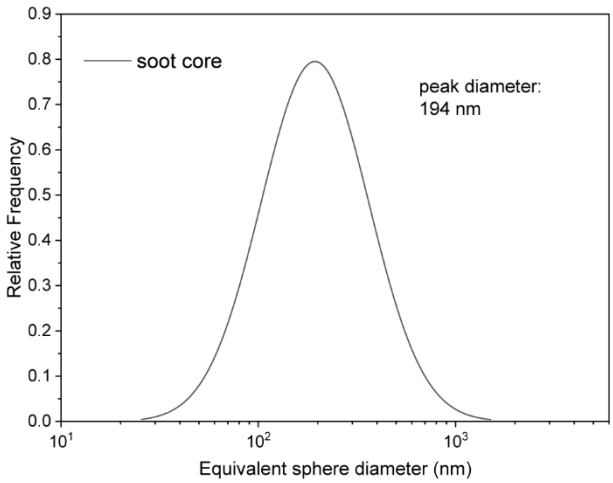

Figure S8. Size distribution of soot cores in individual soot-containing particles.

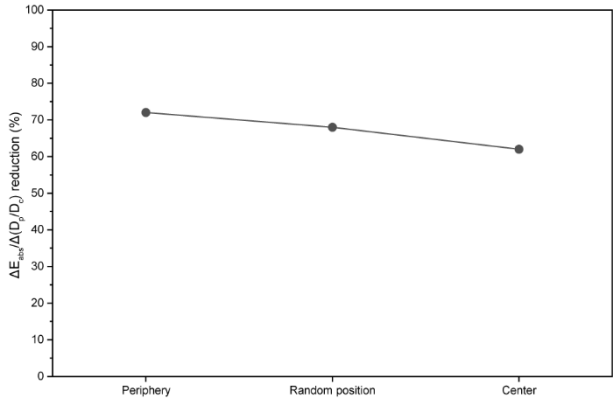

Figure S9. The $\Delta E_{abs}/\Delta(D_p/D_c)$ reduction of transboundary soot-containing particles with different core positions following the transport pathway change from the inland to the sea.

Table S1. The average relative humidity (RH) in the YRD when haze pollutants were transported from the NCP into the YRD through the inland and the sea pathways.

Transport pathway	Average RH
Inland	83%
Sea	90%

Table S2. The mean volume ratio of soot coatings to soot cores ($V_{coating}/V_c$) in two types of transboundary transport models from the NCP to the YRD.

Transport pathway	Region	Particle type	$V_{coating}/V_c$
Inland	NCP	Partly-coated	12
		Embedded	22
	YRD	Partly-coated	21
		Embedded	39
Sea	NCP	Partly-coated	13
		Embedded	24
	YRD	Partly-coated	18
		Embedded	83

Table S3. The change in absorption enhancement simulated by core-shell Mie theory per unit the change in core-shell size ratio ($\Delta E_{abs}/\Delta(D_p/D_c)$) of soot-containing particles during the transboundary transport through the inland and the sea pathways.

Transport pathway	$\Delta E_{abs}/\Delta(D_p/D_c)$
Inland	0.01
Sea	0.03

Supplementary references

Li, W., Sun, J., Xu, L., Shi, Z., Riemer, N., Sun, Y., Fu, P., Zhang, J., Lin, Y., Wang, X., Shao, L., Chen, J., Zhang, X., Wang, Z., and Wang, W.: A conceptual framework for mixing structures in individual aerosol particles, J. Geophys. Res.-Atmos., 121, 13784-13798, https://doi.org/10.1002/2016JD025252, 2016.